Solution Structure of the Aminofluorene [AF]-External Conformer of the *anti*-[AF]-C^8-dG Adduct Opposite dC in a DNA Duplex†

Bing Mao,‡ Brian E. Hingerty,§ Suse Broyde,|| and Dinshaw J. Patel*,‡

Cellular Biochemistry and Biophysics Program, Memorial Sloan Kettering Cancer Center, New York, New York 10021, Health Sciences Research Division, Oak Ridge National Laboratory, Oak Ridge, Tennessee 37831, and Biology Department, New York University, New York, New York 10003

Received September 10, 1997; Revised Manuscript Received October 27, 1997⊗

ABSTRACT: The *Escherichia coli* genome contains a C-G^1-G^2-C-G^3-C-C *Nar*I hot spot sequence for −2 deletion mutations at G^3 by aromatic amine carcinogens 2-acetylaminofluorene (AAF) and 2-aminofluorene (AF) that form covalent adducts at the C^8-position of the guanine ring. Each of the three guanines are positioned in different sequence contexts (C-G^1-G, G-G^2-C, and C-G^3-C) which provides an opportunity to investigate the potential sequence dependent interconversion between AF-intercalated and AF-external conformers of the [AF]dG adduct positioned opposite dC within the *Nar*I sequence at the duplex level. We have prepared and purified DNA duplexes containing the [AF]dG adduct positioned in C-[AF]G-G, G-[AF]G-C, and C-[AF]G-C *Nar*I sequence contexts and observe the ratio of AF-intercalated to AF-external conformers to be 30:70, 10:90, and 50:50, respectively. We have applied a combined NMR-molecular mechanics approach to define the structure of the AF-external conformer in the G-[AF]G-C *Nar*I sequence context where it is the predominant conformation (90%) in solution. The modified guanine of the [AF]dG adduct aligns through Watson−Crick pairing with its partner cytosine and is stacked into the helix between flanking Watson−Crick dG·dC base pairs. The AF-external conformer with its *anti*-[AF]dG residue causes minimal perturbations in the DNA duplex at and adjacent to the lesion site with the covalently linked fluorenyl ring readily accommodated in the major groove and tilted toward the 5′-end of the modified strand of the helix. This paper on the structure of the AF-external conformer with an *anti*-[AF]dG adduct together with the preceding paper in this issue on the structure of the AF-intercalated conformer with a *syn*-[AF]dG adduct defines for the first time the capacity of the mutagenic [AF]dG lesion to adopt interconverting *syn* and *anti* alignments with the equilibrium shifting between the conformers depending on nearest neighbor and next-nearest neighbor sequences. Perhaps, recognition of the [AF]dG lesion by the repair machinery would be able to discriminate between the AF-intercalated conformer with its base displacement-fluorenyl ring insertion perturbation of the helix and the AF-external conformer where the DNA helix is essentially unperturbed at the lesion site and the fluorenyl ring is positioned with directionality in the major groove.

This paper attempts to address the issue of the structural basis of mutagenesis by the chemical carcinogens 2-aminofluorene (AF) and 2-acetylaminofluorene (AAF) at a mutational hot spot sequence in DNA. The d(C-G^1-G^2-C-G^3-C-C) *Nar*I hot spot sequence (*1*−*3*) contains three guanines, each of which can form covalent [AF]dG and [AAF]dG adducts with G^3 as a hot spot for −2 deletions (*2*, *4*−*8*). Previous research has shown that the [AF]dG adduct **1** positioned opposite dC exhibits a slow interconversion between AF-intercalated and AF-external conformers in slow exchange (*9*−*12*). The *Nar*I sequence which contains C-G^1-G, G-G^2-C, and C-G^3-C steps offers a unique opportunity to study the role of nearest neighbor and next-nearest neighbor sequences on the relative populations of AF-intercalated and AF-external conformers of the [AF]dG adduct positioned opposite dC at the duplex level.

The structure of the base displaced-insertion alignment of the AF-intercalated conformer is a matter of dispute with Eckel and Krugh (*9*, *10*) favoring an *anti* alignment at the adducted position and displacement of the modified guanine into the minor groove in the A-[AF]G-G sequence context, while our group established a *syn* alignment at the adducted position and displacement of the modified guanine into the major groove in the C-[AF]G-C sequence context [see preceding paper in this issue (*12*); see also our previous contribution on the aminopyrenyl AP-intercalated conformer of *syn*-[AP]dG positioned opposite dC reported in (ref 13)]. The present study also offers an opportunity to further investigate the generality of NMR parameters associated with the *syn* alignment of the [AF]dG adduct for the AF-

† This research is supported by NIH Grant CA-49982 to D.J.P., by NIH Grants CA-28038, CA-75449, and RR-06458 and DOE Grant DE-FG02-90ER60931 to S.B., and by DOE Contract DE-AC05-960R22464 with Lockheed Martin Energy Research and DOE OHER Field Work Proposal ERKP931 to B.E.H.

* Author to whom correspondence should be addressed.
‡ Memorial Sloan Kettering Cancer Center.
§ Oak Ridge National Laboratory.
|| New York University.

⊗ Abstract published in *Advance ACS Abstracts,* December 15, 1997.

S0006-2960(97)02258-7 CCC: $15.00
Published on Web 01/06/1998

intercalation conformer in different sequence contexts.

The solution structural characterization of the AF-external conformer could be approached provided that this conformer represents the major species in the interconversion between AF-intercalated and AF-external conformers of the [AF]dG adduct positioned opposite dC at the duplex level. This condition has been achieved for adduct formation in the G-[AF]G[2]-C *Nar*I sequence context, and we report on the solution structure of the AF-external conformer in this sequence context.

This paper reports on a comparative study of [AF]dG adducts positioned opposite dC at the 12-mer duplex level where the covalent carcinogenic adduct is positioned at G[1] (designated the [AF]dG4·dC 12-mer duplex **2**, Figure 1B), at G[2] (designated the [AF]dG5·dC 12-mer duplex **3**, Figure 1C), and at G[3] (designated the [AF]dG7·dC 12-mer duplex **4**, Figure 1D) in the *Nar*I hot spot sequence context. The NMR spectra are of good quality for all three adducted duplexes allowing a systematic study of sequence-dependent interconversion between AF-intercalated and AF-external conformers in solution. Further, we report on the solution structure of the AF-external conformer in the [AF]dG5·dC 12-mer duplex.

MATERIALS AND METHODS

Preparation of Adducts. The d(C-T-C-G-G-C-G-C-C-A-T-C) 12-mer sequence was reacted with excess of *N*-acetoxy-2-acetylaminofluorene (AAAF) in 2 mM sodium citrate buffer as described (*14*). Separation of the three monoadducted [AAF]dG isomers was achieved by applying reversed phase HPLC on a C18 ODS-Hypersil semipreparative column (Keystone Scientific, Inc.). The solvent program was an isochratic step at 15% methanol in 20 mM phosphate buffer, pH 7.0 for 10 min, followed by a linear gradient to 40% methanol in 60 min. The pure monoadducted [AAF]-dG isomers were converted into the monoadducted [AF]dG isomers by dissolving in 1 M NaOH containing 0.3% (v/v) 2-mercaptoethanol for 45 min at room temperature, followed by purification using reverse phase HPLC as in the case of the AAF-modified oligomer. The pure [AF]dG isomers were desalted on Sephadex G-25 and converted to sodium form on Dowex 50X8 cation exchange resin. The three AF monoadducted [AF]dG4, [AF]dG5, and [AF]dG7 containing 12-mer oligonucleotides were annealed with the complementary d(G-A-T-G-G-C-G-C-C-G-A-G) 12-mer strand at 70 °C with the stoichiometry followed by monitoring single proton resonances in both strands. NMR analysis confirmed [AF]dG adduct formation in the three duplexes **2**, **3**, and **4**.

NMR Experiments. One and two dimensional NMR spectra were recorded on approximately 6 mg of [AF]dG4·dC 12-mer, [AF]dG5·dC 12-mer, and [AF]dG7·dC 12-mer duplexes and the control 12-mer duplex in 0.6 mL, 0.1 M NaCl, 10 mM phosphate, pH 7.0 aqueous buffer. The NOESY spectrum (150 ms mixing time) of the adduct duplex in H_2O buffer at 1 °C was collected using a jump-return pulse for solvent suppression. NOESY spectra (50, 100, 150, 200, and 300 ms mixing times) were collected to provide NOE buildup data in D_2O buffer at 25 °C.

Further details of NMR data collection and analysis are the same as outlined in the Materials and Methods of the preceding paper in this issue (*12*).

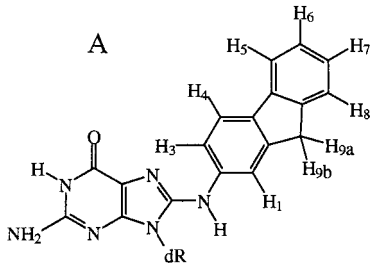

[AF]dG 1

B

C1 – T2 – C3 – G4* – G5 – C6 – G7 – C8 – C9 – A10 – T11 – C12

G24 – A23 – G22 – C21 – C20 – G19 – C18 – G17 – G16 – T15 – A14 – G13

[AF]dG4•dC 12-mer 2

C

C1 – T2 – C3 – G4 – G5* – C6 – G7 – C8 – C9 – A10 – T11 – C12

G24 – A23 – G22 – C21 – C20 – G19 – C18 – G17 – G16 – T15 – A14 – G13

[AF]dG5•dC 12-mer 3

D

C1 – T2 – C3 – G4 – G5 – C6 – G7* – C8 – C9 – A10 – T11 – C12

G24 – A23 – G22 – C21 – C20 – G19 – C18 – G17 – G16 – T15 – A14 – G13

[AF]dG7•dC 12-mer 4

FIGURE 1: Schematic and numbering system of (A) the [AF]dG adduct **1**, (B) the [AF]dG4·dC 12-mer **2**, (C) the [AF]dG5·dC 12-mer **3**, and (D) the [AF]dG7·dC 12-mer **4**.

Molecular Mechanics. The DUPLEX-based molecular mechanics calculations (*15*) are the same as outlined in the Materials and Methods of the preceding paper in this issue (*12*).

RESULTS

Slow Interconversion between AF-Intercalated and AF-External Conformers. The exchangeable imino proton NMR spectra (10.5−14.5 ppm) of the control unmodified *Nar*I sequence containing 12-mer duplex and its [AF]dG substituted counterparts at dG4, dG5, and dG7 in H_2O buffer at 1 °C are plotted in Figure 2. A single conformation is observed for the control unmodified 12-mer duplex (Figure 2A), while two conformers in slow exchange are observed for the three [AF]dG modified duplexes (Figure 2, panels B−D). One of these conformers is of the AF-intercalated type (resolved imino proton assignments designated by the subscript i) since it exhibits the characteristic upfield imino proton shifts for the [AF]dG residue and its flanking base pairs (*9*, *10*, *12*), while the other is of the AF-external type (resolved imino proton assignments designated by the subscript e) based on its minimally perturbed imino proton chemical shifts at and adjacent to the lesion site (*9*−*12*) (Figure 2, panels C and D). A striking feature is the observed sequence dependence of the ratio of the AF-intercalated:AF-external conformers (determined from measurement of imino proton intensities),

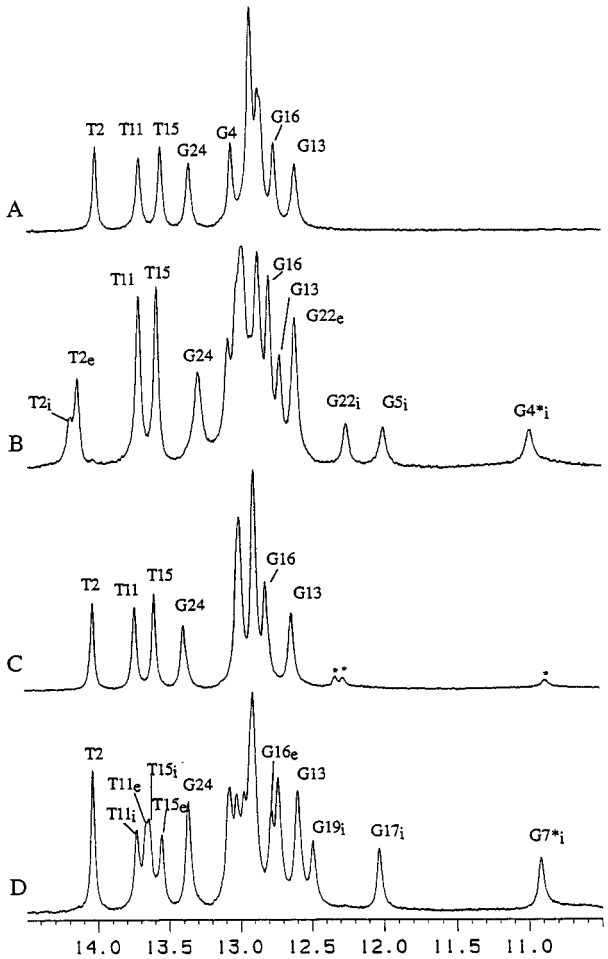

FIGURE 2: Exchangeable imino proton spectra (10.5−14.5 ppm) of (A) control unmodified 12-mer duplex, (B) [AF]dG4·dC 12-mer duplex, (C) [AF]dG5·dC 12-mer duplex, and (D) [AF]dG7·dC 12-mer duplex in H_2O buffer (0.1 M NaCl, 10 mM phosphate, and 0.1 mM EDTA), pH 7.0 at 1 °C. Selective imino proton assignments are recorded over the spectra with subscripts i and e standing for resonances originating in AF-intercalated and AF-external conformers, respectively. Peaks marked with asterisks in panel C are attributed to unassigned imino protons in the AF-intercalated conformer.

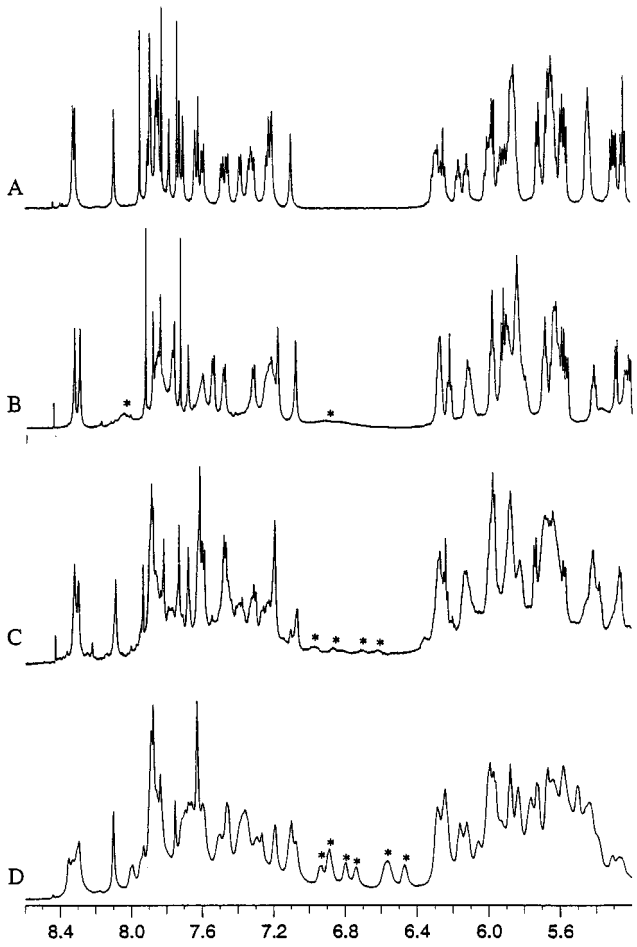

FIGURE 3: Nonexchangeable proton spectra (5.1−8.6 ppm) of (A) control unmodified 12-mer duplex, (B) [AF]dG4·dC 12-mer duplex, (C) [AF]dG5·dC 12-mer duplex, and (D) [AF]dG7·dC 12-mer duplex in D_2O buffer (0.1 M NaCl, 10 mM phosphate, and 0.1 mM EDTA), pH 7.0 at 25 °C. Peaks marked with asterisks in panels B−D represent fluorenyl ring protons in the AF-intercalated conformer.

which varies from 30:70 for the [AF]dG4·dC 11-mer duplex containing a C-[AF]G-G sequence context (Figure 2B) to 10:90 for the [AF]dG5·dC 12-mer duplex containing a G-[AF]G-C sequence context (Figure 2C) to 50:50 for the [AF]dG7·dC 12-mer duplex containing a C-[AF]G-C sequence context (Figure 2D) at 1 °C. The predominance (90%) of the AF-external conformer for the [AF]dG5·dC 12-mer duplex (Figure 2D) should permit a detailed structural characterization of this conformer which in turn should complement our structural characterization of its AF-intercalated counterpart reported in the preceding paper in this issue (*12*).

The base and sugar H1′ nonexchangeable proton NMR spectra (5.2−8.6 ppm) of the control unmodified *Nar*I sequence containing 12-mer duplex, and its [AF]dG substituted counterparts at dG4, dG5, and dG7 in D_2O buffer at 25 °C are plotted in Figure 3. The aromatic [AF]dG fluorenyl protons of the AF-intercalated conformers (designated by asterisks) are shifted upfield into the 6.4−7.0 ppm range and are observed as resolved resonances in the spectra of the adducted duplexes recorded in Figure 3, panels B−D. By contrast, the aromatic [AF]dG fluorenyl protons of the AF-external conformers resonate between 7.4 and 8.0 ppm and are overlapped with the nucleic acid base protons in the spectra of the adducted duplexes. Several of the aromatic fluorenyl protons exhibit chemical shift differences in the 0.8−1.2 ppm range between the AF-intercalated and AF-external conformers of the three [AF]dG·dC adducted duplexes in the *Nar*I sequence context. The line widths of the upfield shifted aromatic fluorenyl protons in the AF-intercalated conformer are dependent on sequence context with somewhat broadened resonances detected for the [AF]-dG7·dC 12-mer duplex containing a C-[AF]G-C sequence context (Figure 3D) and very broad resonances detected for the [AF]dG4·dC 12-mer duplex containing a C-[AF]G-G sequence context (Figure 3B) at 25 °C. However, the fluorenyl protons narrow significantly on lowering the temperature of the [AF]dG4·dC 12-mer duplex sample to 1 °C (Figure S1, Supporting Information).

[AF]dG Adduct in the G-[AF]G-C Sequence Context. The preceding paper in this issue (*12*) reported on the solution structure of the AF-intercalated conformer of [AF]dG positioned opposite dC in the C-[AF]G-C sequence context at the duplex level. This analysis was facilitated by the AF-intercalated conformer being the predominant component

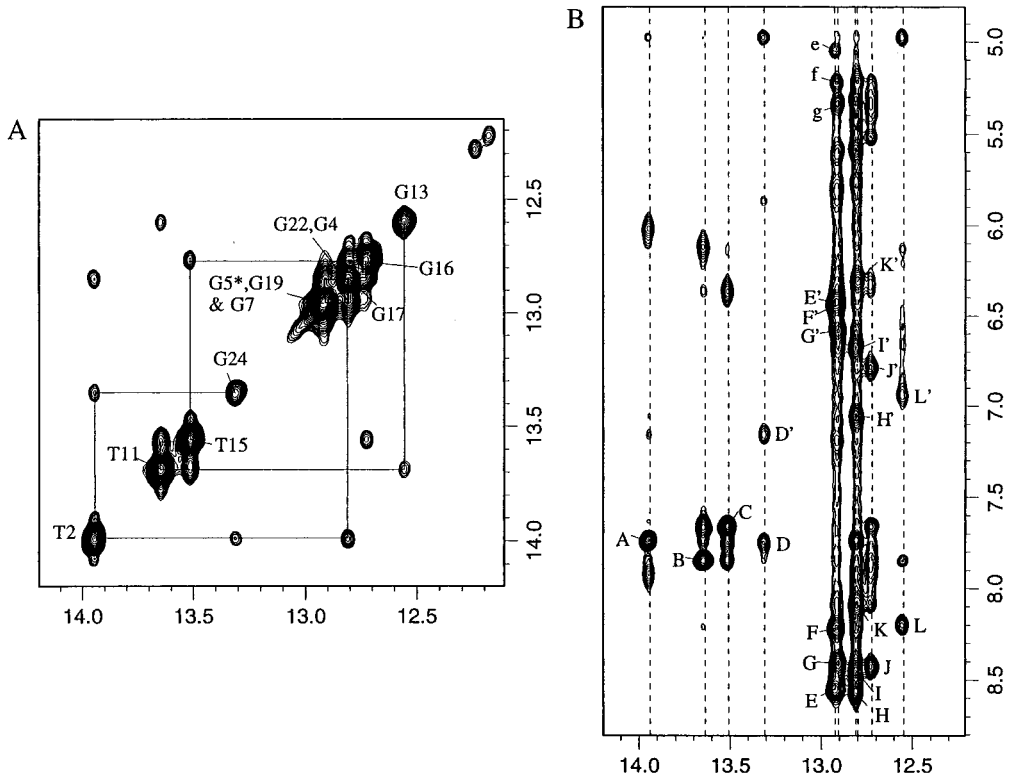

FIGURE 4: Expanded NOESY (150 ms mixing time) contour plots of the [AF]dG5·dC 12-mer duplex in H_2O buffer at 1 °C. (A) NOE connectivities between adjacent base pairs in the symmetrical 12.1−14.2 ppm region are traced starting at dG24 located at one end of the helix and proceeding to dG13 at the other end of the helix (solid line). (B) NOE connectivities between the imino protons (12.2−14.2 ppm) and the nucleic acid base and amino protons and the aminofluorenyl ring protons (4.8−8.8 ppm). The cross-peaks A−C identify thymine imino to adenine H2 protons connectivities across Watson−Crick dA·dT pairs and are assigned as follows: A, dT2(NH3)-dA23(H2); B, dT11(NH3)-dA14(H2), and C, dT15(NH3)-dA10(H2). The cross-peaks D−L identify guanine imino to cytosine amino proton connectivities across Watson−Crick dG·dC pairs and are assigned as follows: D, D′, dG24(NH1)-dC1(NH_2-4b,e); E, E′, dG19(NH1)-dC6(NH_2-4b,e); F, F′, dG7(NH1)-dC18(NH_2-4b,e); G, G′, [AF]dG5(NH1)-dC20(NH_2-4b,e); H, H′, dG22(NH1)-dC3(NH_2-4b,e); I, I′, dG4(NH1)-dC21(NH_2-4b,e); J, J′, dG16(NH1)-dC9(NH_2-4b,e); K, K′, dG17(NH1)-dC8(NH_2-4b,e), and L, L′, dG13(NH1)-dC12(NH_2-4b,e). Cross-peaks e−g are assigned as follows: e, dG19(NH1)-dC6(H5); f, dG7(NH1)-dC18(H5); g, [AF]dG5(NH1)-dC20(H5).

(70%) of the mixture of AF-intercalated and AF-external conformers in slow exchange within this sequence context. Similarly, the structural characterization of the AF-external conformer would be facilitated if it represented the predominant component of the mixture for the [AF]dG adduct positioned opposite dC in a given sequence context. The [AF]dG5·dC 12-mer duplex **3** (Figure 1C) meets this requirement due to the predominance (90%) of the AF-external conformer in the equilibrium (Figure 2C) for this case of the [AF]dG adduct opposite dC in the G-[AF]G-C sequence context. This paper, therefore, focuses on the structural characterization of the AF-external conformer in the [AF]dG5·dC 12-mer duplex. In addition, the contribution also addresses the general issue of the sequence-dependent conformational interconversion between AF-intercalated and AF-external conformers for the three [AF]dG adducts positioned opposite dC in the *Nar*I sequence context.

Exchangeable Nucleic Acid Protons. The exchangeable imino protons of the major conformer in the [AF]dG5·dC 12-mer duplex (Figure 2C) have been assigned from an analysis of expanded NOESY (150 ms mixing time) contour plots in H_2O buffer at 1 °C using established procedures (*16, 17*). We can readily trace the NOE connectivities between imino protons on adjacent base pairs (Figure 4A) and between thymine imino protons and adenine H2 protons across dA·dT base pairs (cross peaks A−C, Figure 4B) and between guanine imino protons and cytosine amino protons across dG·dC base pairs (cross peaks D−L, Figure 4B) in the adduct duplex.

The imino protons of [AF]dG5, dG7, and dG19 are superpositioned at ∼12.93 ppm in the spectrum of the [AF]-dG5·dC 12-mer duplex at 1 °C. Each of them exhibits NOEs to resolved cytosine amino protons across the dG·dC base pairs (peaks labeled E, F, and G, Figure 4B), which in turn exhibit NOEs by spin diffusion to resolved cytosine H5 protons (peaks e, f, and g, Figure 4B). We can distinguish between the imino (and amino) protons of these three guanines since their partner cytosine H5 protons can be assigned independently from an analysis of the nonexchangeable data (see below) on the adduct duplex. Such an analysis yields the chemical shifts of the guanine imino (12.92 ppm) and cytosine amino (6.58 and 8.42 ppm) and H5 (5.04 ppm) protons at the [AF]dG5·dC20 lesion site in the adduct duplex. These results also establish formation of a Watson−Crick [AF]dG·dC pairing alignment which requires that the modified guanine in an *anti* alignment be stacked into the helix in the major conformer of the [AF]dG5·dC 12-mer duplex.

The exchangeable proton chemical shifts for the central d(C3-G4-[AF]G5-C6-G7)·d(C18-G19-C20-C21-G22) segment of the [AF]dG5·dC 12-mer duplex at 1 °C are listed in Table 1 and for the entire duplex in Table S1 (Supporting Information).

Nonexhangeable Nucleic Acid Protons. The nonexchangeable base and sugar protons in the [AF]dG5·dC 12-mer

Table 1: Proton Chemical Shifts of the d(C3-G4-[AF]G5-C6-G7)·d(C18-G19-C20-C21-G22) Segment of the [AF]dG5·dC 12-mer Duplex in Aqueous Buffer

	exchangeable proton chemical shifts (ppm) at 1 °C	
	G(NH1)/T(NH3)	C(NH_2-4)
dC3·dG22	12.82	8.58,[a] 7.05[b]
dG4·dC21	12.82	8.46,[a] 6.68[b]
[AF]dG5·dC20	12.92	8.42,[a] 6.58[b]
dC6·dG19	12.94	8.56,[a] 6.43[b]
dG7·dC18	12.92	8.23,[a] 6.43[b]

	nonexchangeable proton chemical shifts (ppm) at 25 °C				
	H8/H6	H2/H5/CH_3	H1′	H2′, H2″	H3′
dC3	7.41	5.66	5.70	1.94, 2.24	4.75
dG4	7.50		6.00	2.16, 2.57	4.77
[AF]dG5	na		5.83	2.28, 2.54	4.96
dC6	7.21	5.11	5.69	1.94, 2.36	4.81
dG7	7.83		5.88	2.60, 2.70	4.95
dC18	7.25	5.27	5.69	1.94, 2.37	4.81
dG19	7.88		5.95	2.61, 2.80	4.96
dC20	7.34	5.40	5.87	2.10, 2.48	4.74
dC21	7.26	5.37	5.64	1.68, 2.21	4.80
dG22	7.92		5.44	2.71, 2.75	4.97

[a] Hydrogen-bonded amino proton. [b] Exposed amino proton. na not available.

duplex have been assigned based on an analysis of through-space NOESY (300 ms mixing time) and through-bond TOCSY (40 and 80 ms spin lock times) data sets in D_2O solution at 15 and 25 °C using established techniques (reviewed in ref 17). The NOE connectivities between base protons to their own and 5′-flanking sugar H1′ protons have been traced for the central dT2 to dC8 segment on the modified strand (solid lines, Figure 5A) and from dG17 to dA23 segment on the partner unmodified strand (dashed lines, Figure 5A) in the expanded NOESY contour plot of the adduct duplex in D_2O buffer at 15 °C. The interruption in the NOE connectivities for the dG4-[AF]dG5 step on the modified strand (Figure 5A) is due to the absence of a purine H8 proton following covalent aminofluorene modification at the C^8 position of dG5 in the adduct duplex.

Expanded NOESY (100 ms mixing time) and phase sensitive COSY contour plots correlating sugar H1′ protons (5.3−6.4 ppm) with their own sugar H2′,2″ protons (1.6−3.0 ppm) in the [AF]dG5·dC 12-mer duplex in D_2O buffer at 15 °C are plotted in Figure 6. The cross-peaks corresponding to the central d(G4-[AF]G5-C6)·d(G19-C20-C21) segment of the adduct duplex are labeled in Figure 6. The H2′ and H2″ protons were differentiated based on the stronger NOE between the H1′ and H2″ protons relative to the corresponding NOE between the H1′ and H2′ protons in NOESY data sets at short mixing times on the adduct duplex. The chemical shifts of the H2′ and H2″ protons of [AF]-dG5 are 2.28 and 2.54 ppm, respectively, in the [AF]dG5·dC 12-mer duplex.

The nonexchangeable proton chemical shifts for the central d(C3-G4-[AF]G5-C6-G7)·d(C18-G19-C20-C21-G22) segment of the [AF]dG5·dC 12-mer duplex at 15 °C are listed in Table 1 and for the entire duplex in Table S2 (Supporting Information). Exchangeable and nonexchangeable proton chemical shift differences for this central segment between the [AF]dG5·dC 12-mer duplex and the control unmodified 12-mer duplex are listed in Table S3 (Supporting Information).

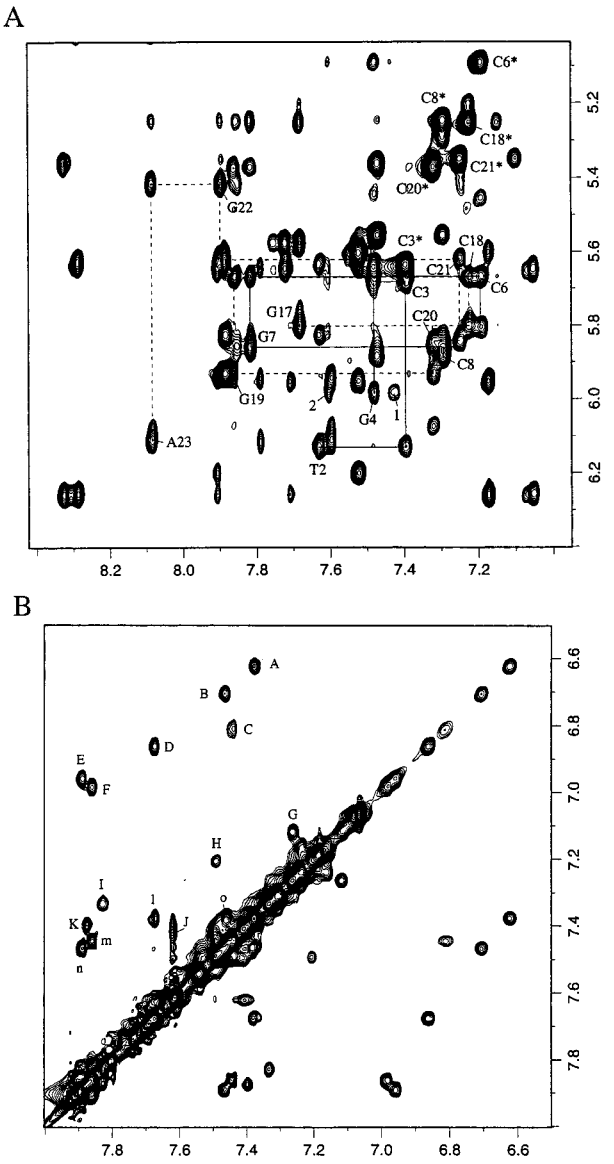

FIGURE 5: (A) Expanded NOESY (300 ms mixing time) contour plot of the [AF]dG5·dC 12-mer duplex in D_2O buffer at 15 °C establishing distance connectivities between the base (purine H8 and pyrimidine H6) protons (7.0−8.4 ppm) and the sugar H1′ and cytosine H5 protons (5.0−6.4 ppm) for the d(T2-C3-G4-[AF]G5-C6-G7-C8)·d(G17-C18-G19-C20-C21-G22-A23) segment. The NOE connectivities between the base and their own and 5′-flanking sugar H1′ protons are traced from dT2 to dC8 on the modified strand (solid line), with the break in connectivity at the dG4 -[AF]dG5 step due to the absence of the H8 proton for [AF]dG5 and from dG17 to dA23 on the unmodified complementary strand (dashed line). The cross-peaks between cytosine H5 and H6 protons are designated by asterisks. The cross-peaks numbered 1 and 2 identify intermolecular AF-DNA NOEs and are assigned as follows: 1, AF-(H3)-dG4(H1′) and 2, AF(H1)-dG4(H1′). (B) Expanded NOESY (100 ms mixing time) contour plots of the [AF]dG5·dC 12-mer duplex in D_2O buffer at 15 °C. Chemical exchange cross-peaks A to K are labeled with capital letters and are assigned as follows: A, AF($H7_{ext}$)-AF($H7_{int}$); B, AF($H6_{ext}$)-AF($H6_{int}$); C, AF($H3_{ext}$)-AF($H3_{int}$); D, AF($H8_{ext}$)-AF($H8_{int}$); E, AF($H5_{ext}$)-AF($H5_{int}$); F, AF($H4_{ext}$)-AF($H4_{int}$); G, dC21($H6_{ext}$)-dC21($H6_{int}$); H, dC6($H6_{int}$)-dC6($H6_{ext}$); I, dC20($H6_{int}$)-dC20($H6_{ext}$); J, AF($H1_{ext}$)-AF($H1_{int}$); K, dG19($H8_{ext}$)-dG19($H8_{int}$). The cross-peaks l−o designate NOEs between AF-external protons and are assigned as follows: l: AF(H8)-AF(H7); m, AF(H4)-AF(H3); n, AF(H5)-AF(H6); o, AF(H6)-AF(H7).

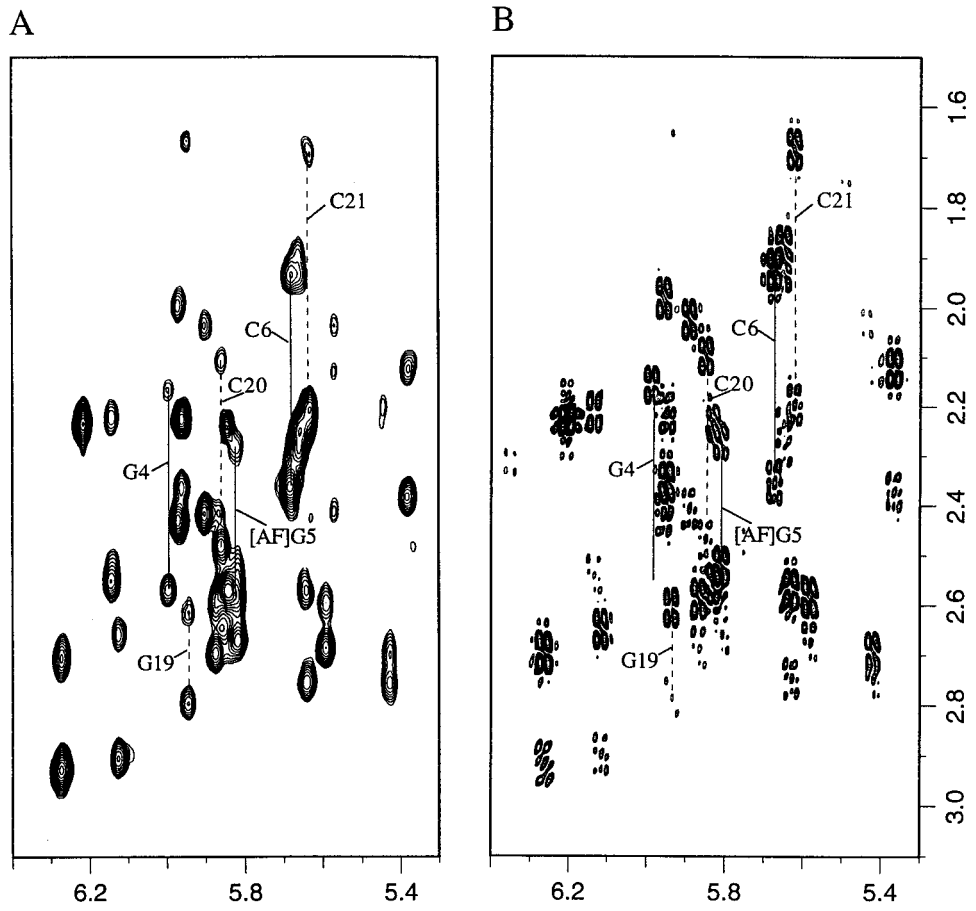

FIGURE 6: (A) An expanded NOESY (100 ms mixing time) contour plot of the [AF]dG5·dC 12-mer duplex in D_2O buffer at 15 °C showing NOE connectivities between the sugar H1′ protons (5.3−6.4 ppm) and H2′, H2″ protons (1.5−3.1 ppm). (B) An expanded phase sensitive COSY contour plot of the [AF]dG5·dC 12-mer duplex in D_2O buffer at 15 °C establishing coupling connectivities between the H1′ protons (5.3−6.4 ppm) and H2′, H2″ protons (1.5−3.1 ppm). In both panels A and B, the H2′ and H2″ protons of dG4, [AF]dG5, dC6, dG19, dC20, and dC21 are connected by lines and labeled. The H2′ protons resonate upfield of the H2″ protons for all these residues including the [AF]dG5 adduct site.

Aminofluorene Protons. The aminofluorenyl ring protons in the major conformer of the [AF]dG·dC 12-mer duplex were assigned from an analysis of NOESY, COSY, and TOCSY data sets in D_2O solution at 15 and 25 °C. In addition, exchange cross-peaks are observed in the expanded NOESY spectrum (100 ms mixing time) between aminofluorenyl ring protons in the major (90%) and minor (10%) conformers of the adduct duplex in D_2O at 15 °C (peaks A−K, Figure 5B) and 25 °C. These chemical shift values in the two conformers are listed in Table 2 with the aromatic aminofluorenyl protons dispersed downfield between 7.4 and 7.9 ppm in the major AF-external conformer and dispersed upfield between 6.6 and 7.3 ppm in the minor AF-intercalated conformer of the [AF]dG5·dC 12-mer duplex at 25 °C. In addition, the AF(NH) proton resonates at 6.80 ppm in the AF-external conformer of the adduct duplex (Table 2).

Intermolecular AF-DNA NOEs. We have observed and identified a set of intermolecular NOEs involving exchangeable (numbered peaks in Figure S2, Supporting Information) and nonexchangeable (numbered peaks in Figure 5A) protons in the [AF]dG5·dC 12-mer duplex. These intermolecular NOEs have been translated into the corresponding AF-DNA distance restraints defined by lower and upper bounds in the adduct duplex and are listed in Table 3.

Carbon Spectra. The expanded contour plot of a natural abundance proton-carbon HMQC correlation experiment that correlates the H1′ and C1′ chemical shifts of individual residues in the [AF]dG5·dC 12-mer duplex in D_2O buffer at 25 °C is plotted in Figure 7A. The carbon resonances are assigned on the basis of the known H1′ proton assignments in the adduct duplex and are labeled in the contour plot (Figure 7A). We note that the C1′ chemical shift of [AF]dG5 (84.5 ppm) falls in the range of other guanine C1′ chemical shifts between 84.0 and 85.0 ppm in the adduct duplex (Figure 7A).

Table 2: Proton Chemical Shift Values (ppm) of the Aminofluorene Ring Protons for the AF-External and AF-Intercalated Conformers in the [AF]dG4·dC 12-mer (1 °C), [AF]dG5·dC 12-mer (25 °C), and [AF]dG7·dC 12-mer (25 °C) Duplexes

	[AF]dG4·dC 12-mer		[AF]dG5·dC 12-mer		[AF]dG7·dC 12-mer	
proton	AF-ext	AF-int	AF-ext	AF-int	AF-ext	AF-int
AF(H1)	7.95	7.67	7.63	7.27	7.69	7.25
AF(H3)	7.52	7.05	7.45	6.79	7.49	7.08
AF(H4)	7.95	6.89	7.87	6.97	7.82	6.91
AF(H5)	7.97	6.76	7.90	6.95	7.85	6.70
AF(H6)	7.52	6.64	7.46	6.70	7.44	6.54
AF(H7)	7.42	6.64	7.38	6.61	7.35	6.53
AF(H8)	7.75	6.87	7.69	6.85	7.64	6.77
AF(H9a,b)	3.85	3.03	3.99	3.09, 3.26	3.94	3.06, 3.20
AF(NH)	na[a]	na	6.80	na	na	na

[a] na, not available.

Table 3: Comparison of Experimental Distance Restraints with Those Observed for the NMR Energy Minimized Structure of the [AF]dG5·dC 12-mer Duplex

	interproton distances (Å)		
	exptl bounds	observed (I)	observed (II)
Exchangeable Protons			
AF(NH)-dG4(H8)	4.0−6.0	5.87	5.55
AF(NH)-dG4(H1′)	3.0−5.0	3.91	3.87
AF(NH)-dG4(H2′)	4.0−6.0	4.14	3.90
AF(NH)-[AF]dG5(H1′)	3.0−5.0	3.83	3.81
AF(NH)-[AF]dG5(H2′)	2.0−4.0	2.48	2.31
AF(NH)-dG4(H2″) and/or [AF]dG5(H2″)[a]	2.5−5.0	2.71, 3.87	2.55, 3.73
AF(NH)-[AF]dG5(H3′)	2.0−4.0	2.93	2.81
Nonexchangeable Protons			
dG4(H1′)-[AF]dG5(H4′)	2.2−4.5	3.95	4.37
dG4(H8)-AF(H1)	2.0−4.0[b]	3.34	5.90
dG4(H1′)-AF(H3)	2.8−5.3	5.44	4.07
dG4(H2′)-AF(H3)	2.1−4.5	4.15	3.08
dG4(H2″)-AF(H1)	2.0−4.0	3.19	3.22
dG4(H2″)-AF(H3)	2.1−3.9	3.29	3.29
dG4(H3′)-AF(H1)	2.8−5.3[c]	5.36	4.77
dG4(H3′)-AF(H3)	2.4−4.5[b]	4.90	5.35
[AF]dG5(H3′)-AF(H3)	3.0−5.6[b]	4.71	6.25
[AF]dG5(H3′)-AF(H1)	2.8−5.2[c]	6.35	4.43
dC6(H5)-AF(H1)	3.0−5.7[c]	6.96	5.01

[a] The resonances of the sugar H2″ protons dG4 and dG5 are overlapped and are given wide experimental bounds. [b] Bounds that are not used in embedding of structure II. [c] Bounds that are not used in embedding of structure I.

Phosphorus Spectra. The proton decoupled phosphorus spectrum of the [AF]dG5·dC 12-mer duplex has been recorded in D_2O buffer at 25 °C. The phosphorus resonances are dispersed between −3.6 and −4.5 ppm and several have been assigned following analysis of a proton-detected phosphorus-proton heteronuclear correlation experiment whose contour plot is shown in Figure 7B. We do not detect unusual upfield or downfield phosphorus resonances for the AF-external conformer of the [AF]dG5·dC 12-mer duplex.

Molecular Mechanics Computations. The search strategy employed began with a cannonical B-DNA (*18*) central d(C3-G4-[AF]G5-C6-G7)·d(C18-G19-C20-C21-G22) base pair segment of the [AF]dG5·dC 12-mer duplex with the molecular mechanics computations guided by the intermolecular AF-DNA restraints listed in Table 3. The DNA starting conformation was the B-form with an *anti* (χ = 245°)-glycosidic torsion angle for [AF]dG5 residue, which was not restricted to this value during the subsequent molecular dynamics calculations. The AF-DNA orientation space was searched with 16 energy minimization trials in which the linkage torsion angles α' [[AF]dG5(N9)-[AF]dG5(C8)-[AF]-(N)-[AF](C2)] and β' [[AF]dG5(C8)-[AF](N)-[AF](C2)-[AF]-(C1)] were each started at 0°, 90°, 180°, and 270° in all combinations, and the DNA starting conformation was B-form. In these trials, the DUPLEX hydrogen-bond penalty function (*15*) for Watson−Crick base pairing was utilized at all base pairs including [AF]dG5·dC20 at the lesion site, since the NMR data indicated that these hydrogen bonds were present along the length of the adduct duplex.

Twelve of the 16 computed structures exhibited good fit to the NMR data and had low energies. These 12 structures were comprised of two different families with views looking into the major groove and normal to the helical axis outlining the superposition within each family of structures are shown in Figure 8. The corresponding energies and goodness-of-fit indices of these 12 structures are listed in Table S4 (Supporting Information). The two families are related by an approximately 180° flip along the β' torsion angle with seven structures (Figure 8A) having the C^9-containing edge pointing toward the 5′-side of the modified strand whereas it points toward the 3′ direction in the other five structures (Figure 8B). The observed pattern of intermolecular AF-DNA NOEs between the protons on different edges of the aminofluorene ring and the central d(G4-[AF]G5-C6) segment define the two rotamer alignments of the aminofluorene ring in the adduct duplex. The AF(H1) proton exhibits an NOE to the base proton of dG4(H8) while the AF(H3) proton exhibits NOEs to the sugar H3′ protons of dG4 and [AF]-dG5 in one alignment (designated I) of the adduct duplex (Table 3). These NOE patterns indicate that the C^9-containing edge of the aminofluorenyl ring is directed toward

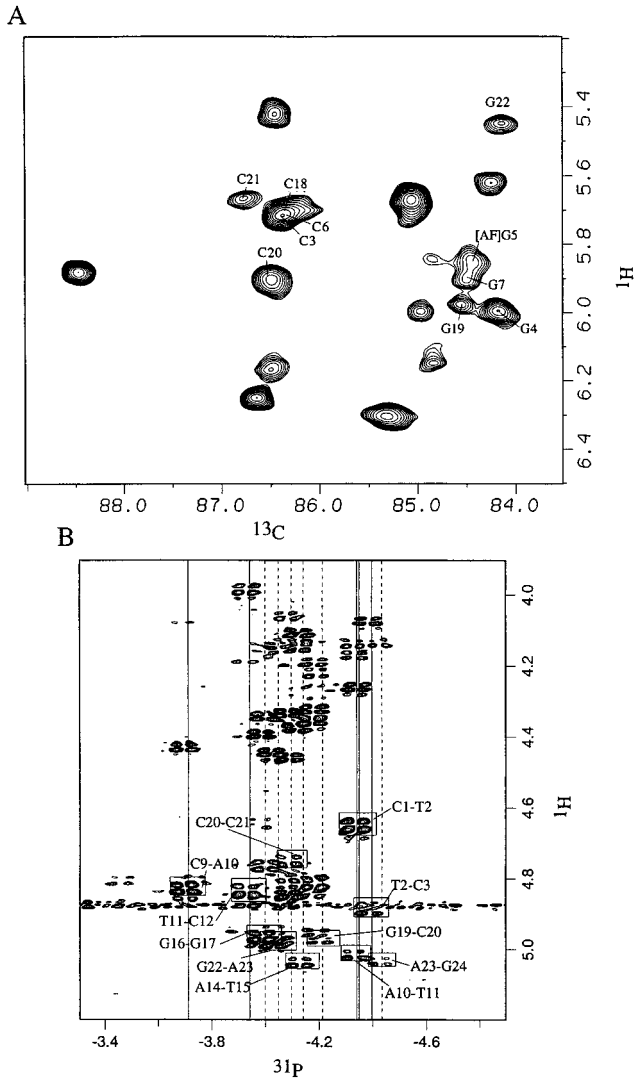

FIGURE 7: (A) An expanded contour-plot of natural abundance ^1H-^{13}C heteronuclear multiple-quantum coherence (HMQC) experiment on the [AF]dG5·dC 12-mer duplex in D_2O buffer at 15 °C. The C1′ assignments for residues in the d(C3-G4-[AF]G5-C6-G7)·d-(C18-G19-C20-C21-G22) segment. (B) An expanded contour-plot of the proton-detected phosphorus-proton heteronuclear correlation experiment on the [AF]dG5·dC 11-mer duplex in D_2O buffer at 15 °C. Several phosphorus assignments are listed in this contour plot. The correlation cross-peaks between the phosphorus and its 5′-flanking sugar H3′ protons are boxed.

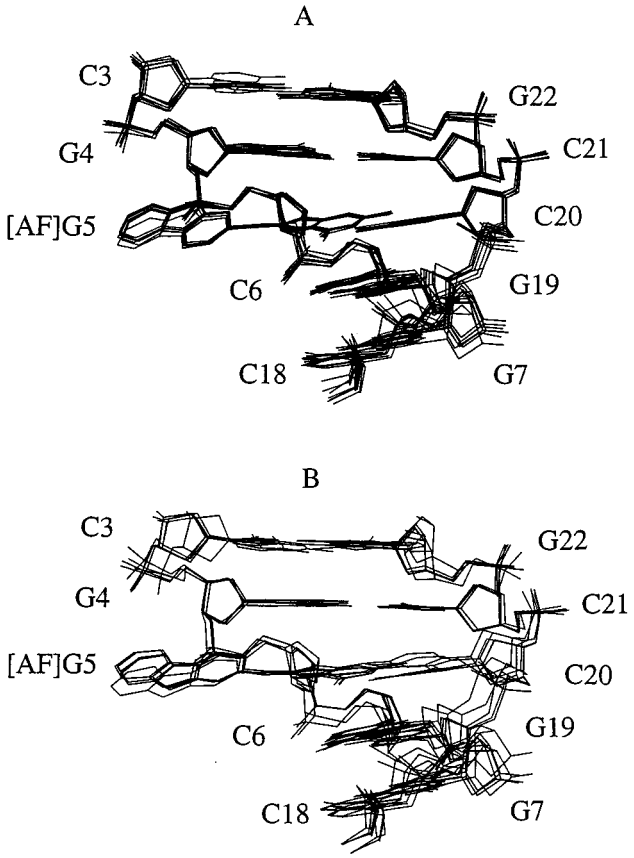

FIGURE 8: View looking into the major groove and normal to the helix axis of the superposition of the twelve d(C3-G4-[AF]G5-C6-G7)·d(C18-G19-C20-C21-G22) 5 base pair segments that best fit the NMR data of the [AF]dG5·dC 12-mer duplex. (A) Seven of 12 structures have the C^9-containing edge of AF pointing toward the 5′-side of the modified strand. (B) Five of 12 structures have the C^9-containing edge of AF pointing toward the 3′-side of the modified strand.

the 5′-side of the modified strand in structure I (Figure 8A) of the adduct duplex. We also observe that the AF(H3) proton exhibits an NOE to the base proton of dC6(H5), while the AF(H1) proton exhibits NOEs to the sugar H3′ protons of dG4 and [AF]dG5 in the other alignment (designated II) of the adduct duplex (Table 3). These NOE patterns indicate that the C^9-containing edge is directed toward the 3′-side of the modified strand in structure II (Figure 8B) of the adduct duplex. Further, these two sets of NOE patterns are also present for the NOESY spectra of the adduct duplex recorded at lower mixing times allowing the exclusion of contributions from spin diffusion effects as an explanation for the observed phenomena. These observations establish the existence of two rotamers in fast exchange on the NMR time scale which are related by 180° flips along the long axis of the aminofluorene ring in the adduct duplex. Two structures with low energy and low values for goodness-of-fit functions (one from each family representing different orientations of AF; structures 2 and 6 in Table S4) were embedded into an energy minimized B-form 11-mer duplex and reminimized with all restraints. Subsequently, the hydrogen-bond penalty function and the distance restraints were released with energy minimization in one step, yielding two final unrestrained structures of the [AF]dG5·dC 12-mer duplex.

Solution Structures of the AF-External Conformer of the [AF]dG5·dC 12-mer Duplex. Views normal to the helix axis and looking into the major groove of the central d(G4-[AF]-G5-C6)·d(G19-C20-C21) segment of the NMR-molecular mechanics structures of the [AF]dG5·dC 12-mer duplex are shown for structure I (C^9-containing edge pointing toward 5′-side) in Figure 9A and for structure II (C^9-containing edge pointing toward 3′-side) in Figure 10A. The covalently linked aminofluorene ring is located in the major groove without disruption of the Watson−Crick hydrogen bonds of the modified base pair in both structures of the adduct duplex. Views looking down the helix axis of the central d(G4-[AF]-G5-C6)·d(G19-C20-C21) segment of the structures of the [AF]dG5·dC 12-mer duplex are shown for structure I in Figure 9B and for structure II in Figure 10B. These views emphasize the overlap geometry between neighboring base pairs centered about the lesion site together with the positioning of the AF ring within the major groove and exposed to solvent.

The carcinogen-base linkage site for the [AF]dG5 residues is defined by the α' and β' torsion angles which adopt values of 200° and 38° in structure I and values of 191° and 213° in structure II of the adduct duplex. The $\beta' = 38°$ orientation directs the C^9-containing edge toward the 5′-side of the modified strand (Figure 9A), while the $\beta' = 213°$ value has the C^9-containing edge directed toward the 3′-side of the modified strand (Figure 10A) for the [AF]dG5·dC 12-mer duplex. The pair of rotamers are related by the 180° rotation about the [AF] long axis that is reflected in the β' values. The glycosidic torsion angles, sugar puckers, and backbone torsion angles for the d(C3-G4-[AF]G5-C6-G7)·d(C18-G19-C20-C21-G22) segment of the [AF]dG5·dC 12-mer duplex are listed for structure I in Table S5 (Supporting Information) and for structure II in Table S6 (Supporting Information). Torsion angles and pseudorotation parameters for structure I and structure II are in or near ranges observed in B-DNA crystals (*19*).

Our attempt to estimate *R* factors, which provide a measure of the quality of the fit between the experimental NMR data and the computed structures, is restricted to the intermolecular NOEs involving nonexchangeable protons for the AF-external conformer (structures I and II) of the [AF]dG5·dC 12-mer duplex listed in Table 3. The experimental intensities were estimated for these intermolecular NOE cross-peaks in the available NOESY data sets recorded at four mixing times and given bound of ±20%. In addition, the intensities of the same intermolecular NOEs at four mixing times were back-calculated based on a relaxation matrix analysis for DUPLEX-refined structures I (Figure 9) and II (Figure 10) of the AF-external conformer of the [AF]dG5·dC 12-mer duplex. A comparision of the experimental and back-calculated intensities gave an *R* value of 3.5% for structure I, which corresponds to the rotomer with the AF C^9 edge directed toward the 5′-end of the modified strand (based on eight intermolecular NOEs excluding those labeled by superscript c in Table 3) and an *R* value of 4.5% for structure II which corresponds to the rotomer with the AF C^9 edge directed toward the 3′-end of the modified strand (based on eight intermolecular NOEs excluding those labeled by superscript b in Table 3). A rotation correlation time of 3.5 ns was used in the back-calculation computations.

NMR Features of the AF-Intercalated Conformer of the [AF]dG7·dC 12-mer Duplex. We have already pointed out that the AF-intercalated conformer of the [AF]dG adduct

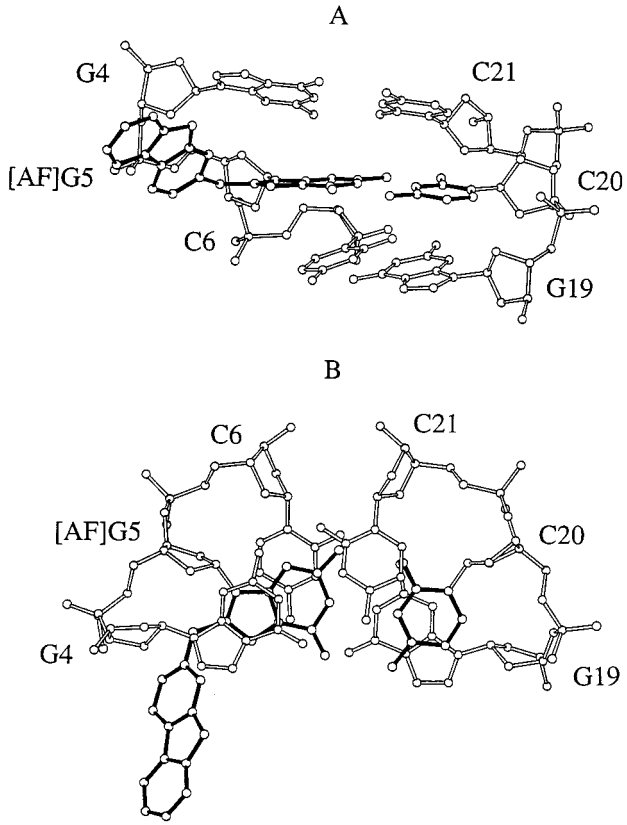

FIGURE 9: (A) View looking into the major groove and normal to the helix axis for the d(G4-[AF]G5-C6)·d(G19-C20-C21) segment of structure I of the [AF]dG5·dC 12-mer duplex. The AF ring system is shown in darkened bonds and is located in the major groove. The Watson−Crick hydrogen-bonding alignment of the modified [AF]dG5·dC20 base pair is shown in darkened bonds. (B) View looking down the helix axis for the d(G4-[AF]G5-C6)·d(G19-C20-C21) segment of structure I of the [AF]dG5·dC 12-mer duplex. Note that the C^9-containing edge is pointing toward the 5′-side of the modified strand. Figures were prepared using Molscript V1.1 (*32*).

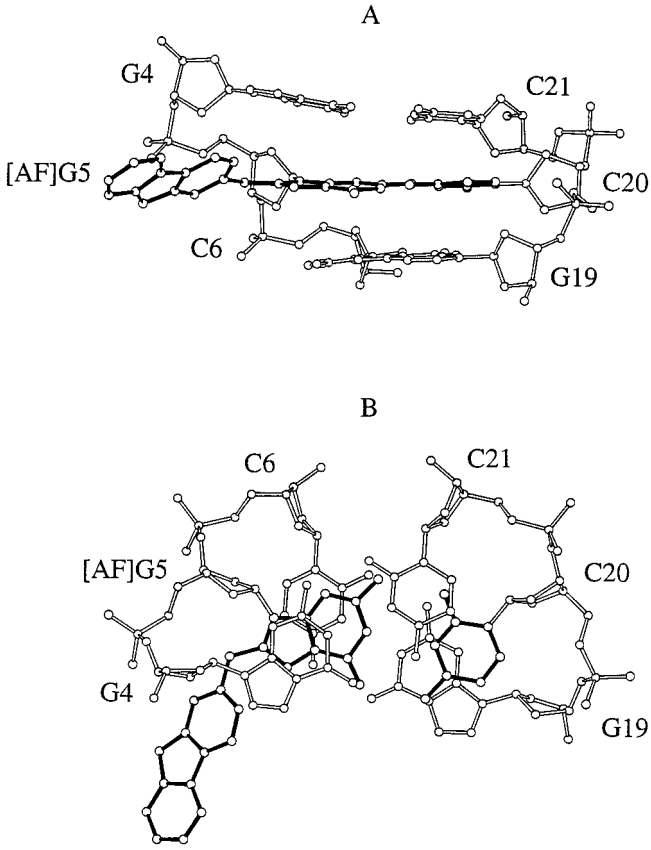

FIGURE 10: (A) View looking into the major groove and normal to the helix axis for the d(G4-[AF]G5-C6)·d(G19-C20-C21) segment of structure II of the [AF]dG5·dC 12-mer duplex. The AF ring system is shown in darkened bonds and is located in the major groove. The Watson−Crick hydrogen bonding alignment of the modified [AF]dG5·dC20 base pair is shown in darkened bonds. (B) View looking down the helix axis for the d(G4-[AF]G5-C6)·d(G19-C20-C21) segment of structure II of the [AF]dG5·dC 12-mer duplex. Note that the C^9-containing edge is pointing toward the 3′-side of the modified strand. Figures were prepared using Molscript V1.1 (*32*).

positioned opposite dC can be distinguished from its AF-external counterpart based on the upfield proton chemical shifts of the exchangeable imino protons of the [AF]dG adduct and its flanking base pairs (Figure 2) and the upfield chemical shifts of the nonexchangeable fluorenyl ring protons (Figure 3). The population of the AF-intercalated conformer is 30% for the [AF]dG4·dC 12-mer duplex containing a C-[AF]G-G sequence context (Figure 2B) and is 50% for the [AF]dG7·dC 12-mer duplex containing a C-[AF]G-C sequence context (Figure 2D). We summarize below additional chemical shift patterns that are characteristic of AF-intercalated conformers for [AF]dG adducts positioned opposite dC at the duplex level.

An expanded NOESY (100 ms mixing time) contour plot correlating NOEs between the base protons (5.3−6.7 ppm) and the sugar H1′ protons (1.4−3.8 ppm) of the [AF]dG7·dC 12-mer duplex is plotted in Figure 11. The sugar H2′ proton of the [AF]dG7 adduct (3.71 ppm) undergoes a large downfield shift for the AF-intercalated conformer in the adduct duplex. Such a large downfield shift of the sugar H2′ proton of the adducted guanine has been shown to be a signature for a *syn* alignment at the modified guanine (*20*) consistent with the adducted guanine adopting a *syn*-glycosidic torsion angle in the AF-intercalation conformer of the [AF]dG7·dC 12-mer duplex. Note also that the H2′ proton of C6 (1.50 ppm), which is the residue 5′ to the adducted guanine, shifts to high field in the adduct duplex. This has been previously shown to reflect the stacking of the displaced purine ring of the adducted guanine over the major groove base and sugar edge of its 5′-neighboring residue in AF-intercalated conformers of the adduct duplex (*13*, *21*−*22*).

We have also compiled the fluorenyl proton chemical shifts in the AF-intercalated and AF-external conformers of the [AF]dG4·dC 12-mer and [AF]dG7·dC 12-mer duplexes following identification of exchange cross-peaks in NOESY spectra of the adduct duplexes. These values are listed in Table 2 with the fluorenyl protons resonating to higher field in the AF-intercalated conformer relative to the AF-external conformer for both adduct duplexes.

DISCUSSION

AF-External Conformer. The structure of the AF-external conformer has been determined from an NMR-molecular mechanics study of the [AF]dG5·dC 12-mer duplex **3** (Figure 1C). The [AF]dG5 adduct in an *anti* orientation about the glycosidic bond aligns through Watson−Crick pairing with its partner dC20 at the lesion site. The AF ring is positioned

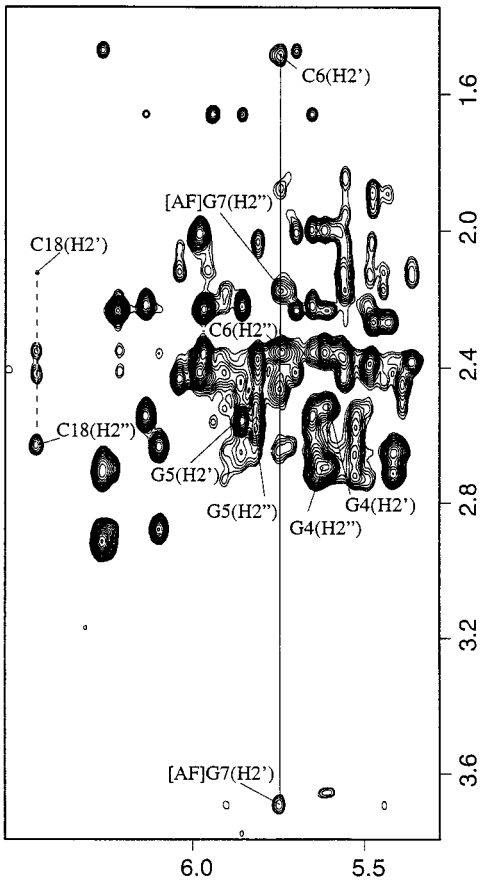

FIGURE 11: An expanded NOESY (100 ms mixing time) contour plot of the [AF]dG7·dC 12-mer duplex in D_2O buffer at 25 °C showing NOE between the sugar H1′ protons (5.3−7.0 ppm) and H2′, H2″ protons (1.4−3.8 ppm). The H2′ and H2″ protons of dG4, dG5, dC6, [AF]dG7, and dC18 are connected by lines and labeled. The H2′ protons resonate upfield of the H2″ protons for these residues except for the [AF]dG7 residue. The H2′ of [AF]dG7 exhibits a chemical shift of 3.70 ppm.

in the major groove and interconverts between two rotamer orientations that are related by rapid 180° flips along the β' torsion angle (Figures 9 and 10). We observe only nominal chemical shift differences between the control unmodified 12-mer duplex and the AF-external conformer of the [AF]-dG5·dC 12-mer duplex consistent with minimal perturbation of the B-form DNA helix at and adjacent to the covalent adduct site (Figures 9 and 10).

Our AF-external conformer involving [AF]dG adduct formation at site G^2 (representing the G-[AF]G-C sequence context) in the *Nar*I hot spot sequence at the 12-mer level is similar to that reported by Eckel and Krugh (*9, 10*) for the AF-external conformer in the c-H-*ras* 1 protooncogene sequence (representing the A-[AF]G-G sequence context) at the 10-mer level. Our structure of the AF-external conformer was based on 17 intermolecular NOEs under conditions where the equilibrium between AF-external and AF-intercalated conformers was heavily weighted (90%) toward the former conformer. The structure determination of the AF-external conformer in the Eckel and Krugh (*9, 10*) study was based on three intermolecular NOEs with equal populations of the AF-external and AF-intercalated conformers in equilibrium.

An important difference between our study and that of Eckel and Krugh (*9, 10*) concerns the chemical shift of the H2′ proton of [AF]dG in the AF-external conformer. We observe an upfield shift of 0.21 ppm for this proton on proceeding from the control duplex to the adducted duplex while Eckel and Krugh (*9, 10*) report a large downfield of 0.90 ppm for this proton on adduct formation. It is conceivable that the sugar H2′ chemical shift of [AF]dG assigned by Eckel and Krugh (*9, 10*) to the AF-external conformer may actually originate in the equally populated AF-intercalated conformer for which characteristic large downfield shifts have been observed for this proton for several systems reported from our laboratory (*12, 13, 21*−*23*).

AF-Intercalated Conformer. The characteristic NMR features of the AF-intercalated conformer for [AF]dG positioned opposite dC are severalfold and are summarized below: these include (1) large upfield shifts of the imino protons of the [AF]dG adduct and its flanking base pairs, (2) large upfield shifts of the aromatic fluorenyl ring protons, (3) large downfield shift of the H2′ proton of the [AF]dG adduct site, and (4) upfield shift of the H2′ proton of the residue on the 5′-side of the [AF]dG adduct site. These shifts reflect intercalation of the fluorenyl ring into the helix between intact neighboring base pairs and displacement of the *syn* modified guanine into the major groove (*12, 13*).

The AF-intercalated conformer is populated to the extent of 30% on modification of the G^1 *Nar*I site (representing the C-[AF]G-G sequence context as observed in the [AF]-dG**4**·dC 12-mer duplex **2**) and populated to the extent of 50% on modification of the G^3 *Nar*I site (representing the C-[AF]G-C sequence context as observed in the [AF]dG7·dC 12-mer duplex **4**). The AF-intercalated conformers of [AF]dG adducts at *Nar*I G^1 and G^3 hot spot sites satisfy the criteria listed above.

We reemphasize that the large downfield shift of the H2′ proton of [AF]dG in the AF-intercalated conformer is a key marker for identifying *syn*-glycosidic torsion angles at the adducted residue. The sugar H2′ proton of *syn*-[AF]dG in the AF-intercalated conformers resonates at 3.70 ppm in the [AF]dG7·dC 12-mer duplex (Figure 11) and at 3.71 ppm in the [AF]dG·dC 11-mer duplex reported in the preceding paper in this issue (*12*). These downfield shifts must reflect the in-plane deshielding ring current contributions by the base displaced modified guanine positioned in the major groove of the helix on its own H2′ proton.

Sequence Dependence of Conformer Equilibrium. The slow interconversion between AF-intercalated and AF-external conformers in equilibrium is dependent to a significant degree on nearest neighbor sequence context as readily demonstrated for incorporation of the [AF]dG adduct at the three guanine sites in the *Nar*I sequence context. The stacking patterns centered about the lesion site for the d(N1-[AF]G-N2)·d(N3-C-N4) sequence context in the structure of the AF-intercalated conformer deduced in the preceding paper in this issue (*12*) establishes that residues N2, N3, and N4 (but not N1) stack well with the intercalated AF aromatic ring system. It is therefore not surprising (given that purine rings have a larger surface area for stacking compared to pyrimidine rings) that the largest fraction of the AF-intercalated conformer (50%) is observed for the d(C-[AF]G-C)·d(G-C-G) sequence context in the [AF]dG7·dC 12-mer duplex where N2 is a cytosine and N3 and N4 on the partner strand are guanine residues. The smallest fraction (10%) of

AF-intercalated conformer is observed for the (G-[AF]G-C)•(G-C-C) sequence context in the [AF]dG5•dC 12-mer duplex where N2 and N4 are cytosine residues while N3 is a guanine residue.

It should be noted that next-nearest neighbor sequence effects also influence the distribution between AF-intercalated and AF-external conformers in equilibrium for the [AF]dG adduct positioned opposite dC at the duplex level. Thus, the 50 % population of the AF-intercalated conformer observed for the G-C-[AF]G-C-C sequence context in the [AF]dG7•dC 12-mer duplex reported in this study increases to a 70% population of the AF-intercalated conformer for the T-C-[AF]G-C-T sequence context in the [AF]dG•dC 11-mer duplex reported in the preceding paper in this issue (*12*). It is likely that next-nearest neighbors also modulate the biological activities of these covalent carcinogenic lesions as has been demonstrated for AAF mutagenesis in the *Nar*I sequence following modification at the G^3 site in this hot spot sequence (*24*).

Conformer Interconversion. The fluorenyl protons exhibit distinct chemical shifts for the AF-intercalated and AF-external conformers with the largest chemical shift differences ranging up to 1.2 ppm for all three [AF]dG adducts opposite dC in the *Nar*I sequence context (Table 2). The observation of exchange cross-peaks in NOESY spectra (Figure 5B) implies that exchange is slow relative to the 1.2 ppm (720 Hz at 600 MHz) chemical shift difference. However, the broader line widths of the fluorenyl protons in the [AF]dG4•dC 12-mer duplex (Figure 3B) translates into faster interconversion rates relative to the [AF]dG7•dC 12-mer duplex (Figure 3D). These observations establish a dependence on flanking sequence for the interconversion rates between AF-intercalated and AF-external conformers for [AF]dG adducts opposite dC in the *Nar*I sequence context.

Biological Implications. Our research has demonstrated that the [AF]dG adduct positioned opposite dC can adopt both *syn* (AF-intercalated conformer) and *anti* (AF-external conformer) alignments and that this equilibrium is dependent on both nearest neighbor and next-nearest neighbor sequence contexts. By contrast, [AAF]dG adducts positioned opposite dC appear to strongly prefer *syn* alignments in structures deduced from computations (*25*−*27*) and from NMR studies (*28*). This difference may well account for modulations in susceptibility to repair of [AAF]dG adducts. It is plausible that the [AAF]dG adduct is more prone to repair (reviewed in ref 29) because of its much greater propensity to adopt the abnormal *syn* conformation. In addition, AAF's much greater propensity than AF to act as a polymerase block (reviewed in refs 30 and 31) may also be related to this difference. Furthermore, the [AF]dG adduct is generally bypassed by polymerase when the lesion is positioned at G^1 and G^2 but not G^3 within the *Nar*I hot spot site (*2*). This may reflect the lower population of the structurally disruptive AF-intercalated conformer for the [AF]dG adduct positioned at G^1 (30%) and G^2 (10%) sites relative to the G^3 (50%) site in the *Nar*I hot spot sequence. Analogous sequences dependent differences in repair could also be anticipated from these structural differences.

Coordinates. The coordinates of the *anti* AF-external conformer of the [AF]dG•dC 11-mer are available on request from S.B., whose email address is broyde@nyu.edu.

ACKNOWLEDGMENT

We thank Marazban Dehnugara for his technical assistance and Zengtian Gu for helpful discussions on this project.

SUPPORTING INFORMATION AVAILABLE

Six tables listing the complete exchangeable and nonexchangeable proton chemical shifts for the [AF]dG5•dC 12-mer duplex, chemical shift differences between the [AF]-dG5•dC 12-mer duplex and control unmodified 12-mer duplex, energy and goodness-of-fit parameters of 12 structures and the backbone torsion angles for the central 5-mer segment and two figures outlining the temperature dependence of the nonexchangeable proton spectra of the [AF]-dG4•dC 12-mer duplex, and an expanded NOESY contour plot of the [AF]dG5•dC 12-mer duplex (11 pages). Ordering information is given on any current masthead page.

REFERENCES

1. Fuchs, R. P. P., Schwartz, N., and Daune, M. P. (1981) *Nature, 294*, 657−659.
2. Belguise-Valladier, P., and Fuchs, R. P. P. (1995) *J. Mol. Biol. 249*, 903−913.
3. Milhé, C., Fuchs, R. P. P., and Lefevre, J. -F. (1996) *Eur. J. Biochem. 235*, 120−127.
4. Fuchs, R. P. P. (1983) *J. Mol. Biol. 177*, 173−180.
5. Bichara, M., and Fuchs, R. P. P. (1985) *J. Mol. Biol. 183*, 341−351.
6. Burnouf, D., Koehl, P., and Fuchs, R. P. P. (1989) *Proc. Natl. Acad. Sci. U.S.A. 86*, 4147−4151.
7. Melchior, W. B., Jr., Marques, M. M., and Beland, F. A. (1994) *Carcinogenesis 15*, 889−899.
8. Tebbs, R. -S., and Romano, L. J. (1994) *Biochemistry 33*, 8998−9006.
9. Eckel, L. M., and Krugh, T. R. (1994) *Nat. Struct. Biol. 1*, 89−94.
10. Eckel, L. M., and Krugh, T. R. (1994) *Biochemistry 33*, 13611−13624.
11. Cho, B. P. Beland, F. A., and Marques, M. M. (1994) *Biochemistry 33*, 1373−1384.
12. Mao, B., Hingerty, B. E., Broyde, S., and Patel, D. J. (1998) *Biochemistry 37*, 81−94.
13. Mao, B., Vyas, R. R., Hingerty, B. E., Broyde, S., Basu, A. K., and Patel, D. J. (1996) *Biochemistry 35*, 12659−12670.
14. Koehl, P., Valladier, P., Lefevre, J. F., and Fuchs, R. P. P. (1989) *Nucleic Acids Res. 17*, 9531−9541.
15. Hingerty, B. E., Figueroa, S., Hayden, T., and Broyde, S. (1989) *Biopolymers 28*, 1195−1222.
16. Patel, D. J., Shapiro, L., and Hare, D. (1987) *Annu. Rev. Biophys. Chem. 16*, 423−454.
17. van der Ven, F. J., and Hilbers, C. W. (1988) *Eur. J. Biochem. 178*, 1−38.
18. Arnott, S., Bond, P. J., Selsing, E., and Smith, P. J. (1976) *Nucleic Acids Res. 2*, 2459−2470.
19. Berman, H. M., Olson, W. K., Beveridge, D. L., Westbrook, J., Gelbin, A., Demeny, T., Hsieh, S. H., Srinivasan, A. R., and Schneider, B. (1992) *Biophys. J. 63*, 751−759.
20. Cosman, M., Hingerty, B. E., Geacintov, N. E., Broyde, S., and Patel, D. J. (1995) *Biochemistry 34*, 15334−15350.
21. Mao, B., Cosman, M., Hingerty, B. E., Broyde, S., and Patel, D. J. (1995) *Biochemistry 34*, 6226−6238.
22. Mao, B., M., Hingerty, B. E., Broyde, S., and Patel, D. J. (1995) *Biochemistry 34*, 16641−16653.
23. Norman, D., Abuaf, P., Hingerty, B. E., Live, D., Grunberger, D., Broyde, S., and Patel, D. J. (1989) *Biochemistry 28*, 7462−7476.
24. Belguise-Valladier, P., and Fuchs, R. P. P. (1991) *Biochemistry 30*, 10091−10100.

25. Hingerty, B. E., and Broyde, S. (1982) *Biochemistry 21*, 3243−3252.
26. Lipkowitz, K. B., Chevalier, T., Widdifield, M., and Beland, F. A. (1982) *Chem.-Biol. Interact. 40*, 57−76.
27. Shapiro, R., Sidawi, D., Miao, Y. S., Hingerty, B. E., Schmidt, K. E., Moskowitz, J., and Broyde, S. (1994) *Chem. Res. Toxicol. 7*, 239−253.
28. O'Handley, F. F., Sanford, D. G., Xu, R., Lester, C. C., Hingerty, B. E., Broyde, S., and Krugh, T. R. (1993) *Biochemistry 32*, 2481−2497.
29. Koffel-Schwartz, N., and Fuchs, R. P. P. (1995) *J. Mol. Biol. 252*, 507−513.
30. Heflich, R. H., and Neft, R. E. (1994) *Mutat. Res.: Rev. Genet. Toxicol. 318*, 73−174.
31. Doisy, R., and Tang, M.-S. (1995) *Biochemistry 34*, 4358−4368.
32. Kraulis, P. J. (1991) *J. Appl. Crystallogr. 24*, 946−950.
33. Altona, C., and Sundaralingam, M. (1972) *J. Am. Chem. Soc. 94*, 8205−8212.

BI972258G